

## Surface reconstructions and surface energies of monolayer-coverage cation-terminated Ga<sub>0.5</sub>In<sub>0.5</sub>P(001) surfaces

Sverre Froyen and Alex Zunger

Citation: *Journal of Vacuum Science & Technology B* **9**, 2176 (1991); doi: 10.1116/1.585760

View online: <http://dx.doi.org/10.1116/1.585760>

View Table of Contents: <http://scitation.aip.org/content/avs/journal/jvstb/9/4?ver=pdfcov>

Published by the AVS: Science & Technology of Materials, Interfaces, and Processing

### Articles you may be interested in

[Carrier localization effects in energy up conversion at ordered \(Al 0.5 Ga 0.5 \) 0.5 In 0.5 P/GaAs heterointerface](#)  
*J. Appl. Phys.* **84**, 359 (1998); 10.1063/1.368036

[Scanning tunneling microscopy study of reconstruction of 0.8 monolayers Ga on an Si \(001\) surface](#)  
*J. Vac. Sci. Technol. B* **16**, 645 (1998); 10.1116/1.589874

[Real-time investigation of In surface segregation in chemical beam epitaxy of In<sub>0.5</sub>Ga<sub>0.5</sub>P on GaAs \(001\)](#)  
*Appl. Phys. Lett.* **68**, 3579 (1996); 10.1063/1.116643

[Annealing-induced near-surface ordering in disordered Ga<sub>0.5</sub>In<sub>0.5</sub>P](#)  
*J. Vac. Sci. Technol. B* **13**, 1755 (1995); 10.1116/1.587808

[Ordering of Al<sub>0.5</sub>Ga<sub>0.5</sub>P by high-energy electron irradiation](#)  
*Appl. Phys. Lett.* **53**, 1596 (1988); 10.1063/1.99922



## Instruments for Advanced Science

<p>Contact Hiden Analytical for further details:  <b>W</b> <a href="http://www.HidenAnalytical.com">www.HidenAnalytical.com</a>  <b>E</b> <a href="mailto:info@hiden.co.uk">info@hiden.co.uk</a></p> <p><a href="#">CLICK TO VIEW</a> our product catalogue</p>	 <p><b>Gas Analysis</b></p> <ul style="list-style-type: none"> <li>› dynamic measurement of reaction gas streams</li> <li>› catalysis and thermal analysis</li> <li>› molecular beam studies</li> <li>› dissolved species probes</li> <li>› fermentation, environmental and ecological studies</li> </ul>	 <p><b>Surface Science</b></p> <ul style="list-style-type: none"> <li>› UHV TPD</li> <li>› SIMS</li> <li>› end point detection in ion beam etch</li> <li>› elemental imaging - surface mapping</li> </ul>	 <p><b>Plasma Diagnostics</b></p> <ul style="list-style-type: none"> <li>› plasma source characterization</li> <li>› etch and deposition process reaction</li> <li>› kinetic studies</li> <li>› analysis of neutral and radical species</li> </ul>	 <p><b>Vacuum Analysis</b></p> <ul style="list-style-type: none"> <li>› partial pressure measurement and control of process gases</li> <li>› reactive sputter process control</li> <li>› vacuum diagnostics</li> <li>› vacuum coating process monitoring</li> </ul>
---	--	--	--	--

# Surface reconstructions and surface energies of monolayer-coverage cation-terminated $\text{Ga}_{0.5}\text{In}_{0.5}\text{P}$ (001) surfaces

Sverre Froyen and Alex Zunger  
Solar Energy Research Institute, Golden, Colorado 80401

(Received 29 January 1991; accepted 10 April 1991)

Using the first-principles pseudopotential method we have studied the fully covered cation-terminated (001) surfaces of  $\text{Ga}_{0.5}\text{In}_{0.5}\text{P}$  alloys. We find that among several possible Ga and In surface patterns (within a  $2 \times 2$  unit cell), the one corresponding to CuPt-like bulk ordering is stabilized by  $\sim 100$  meV per surface atom. This structure has been observed experimentally in thick films, yet is known to be bulk unstable. The stability of a CuPt-like surface layer is related to electronically driven surface reconstructions—dimerization, buckling, and tilting—which are discussed in detail.

## I. INTRODUCTION

The polar (001) surfaces of III-V semiconductors show a multitude of surface reconstructions as the stoichiometry of the surface is varied.<sup>1</sup> For example, the (001) surface of GaAs undergoes a series of reconstructions with the symmetries  $c(4 \times 4)$ ,  $c(2 \times 8)$ ,  $1 \times 6$ ,  $4 \times 6$ , and  $c(8 \times 2)$  as the surface changes from As rich to Ga rich. The various reconstructions are generally believed to be formed by Ga-Ga or As-As dimers attached to the surface in various patterns and densities.<sup>1</sup> The pattern changes with Ga/As ratio because the surface prefers to be electronically self-compensated, i.e., with all As dangling bond states filled and all Ga dangling bond states empty.<sup>2</sup> The surfaces of other III-V compounds are less well studied but there are indications<sup>3</sup> that they possess similar reconstructions. Simple dimerized (001) surfaces terminated by a full monolayer of either the group III element or the group V element contain only one type of dangling bonds and should therefore be precluded by the self-compensation requirement. Such surfaces have an odd number of electrons per dimer leading to half-filled bands and metallic surfaces. Still, surface calculations by Qian *et al.*<sup>4</sup> show that the energy of the monolayer-coverage (metallic) Ga-terminated GaAs surface is similar to that of the half-monolayer covered surface with the excess Ga as bulk Ga metal. They argue, however, that orbital rehybridizations, allowed in larger surface unit cells, will cause additional stabilization of the half-monolayer surface. The first question we address is whether there exist reconstruction modes also for monolayer-coverage cation-terminated III-V (001) surfaces that allows compensation and give rise to finite band gap. We describe a novel reconstruction mode which significantly lower the surface energy compared to the simple dimerized surface and also produces a semiconducting surface.<sup>5</sup> This is accomplished by modifications in the dimer geometry, i.e., dimer buckling and tilting. The gap is caused by a symmetry breaking between otherwise equal dimers with an attendant electron transfer between dimers rather than the cation/anion transfer found in the partially covered surfaces. These novel reconstructions lower the surface energy by 50–200 meV per surface atoms relative to the a surface with simple dimers.

The above considerations apply to binary III-V semiconductors. For pseudobinary semiconductor alloys,  $A_{0.5}B_{0.5}C$ , in addition to surface reconstruction and stoichiometry, there are new topological possibilities associated with the two-dimensional pattern or structure of *A* and *B* atoms on the surface. For a dimerized surface, for instance, this might lead to dimers that are of type *A*—*A*, *A*—*B*, or *B*—*B*. If a single pattern is more stable than others, we would expect alloy surface ordering, conceivably in a structure which is different than the one stable in the bulk alloy. This has been observed in metal alloys.<sup>6</sup> If two or more surface patterns have similar energies we would expect a disordered surface. The second question we address is the energetic consequences of these new alloy degrees of freedom.

This was the basic premise behind a suggestion by Suzuki *et al.*<sup>7</sup> who postulated that surface ordering at a cation terminated (001) surface of  $\text{Ga}_{0.5}\text{In}_{0.5}\text{P}$  could give rise to the CuPt-like (CP) ordering which is observed in  $\text{GaInP}_2$  (bulk) films grown by gas-phase epitaxy.<sup>8</sup> Even among homogeneous bulk structures, this structure, which is a  $(\text{GaP})_1(\text{InP})_1$  superlattice in the  $[111]$  direction, is not the lowest energy bulk structure<sup>9,10</sup> and should therefore not be seen if bulk energetics were responsible for the observed ordering. Suzuki *et al.*<sup>7</sup> originally suggested that the surface ordering was caused by elastic surface relaxations driven by the size mismatch between Ga and In. Calculations show that the energy differences between the various competing cation topologies are too small,<sup>5,11</sup> however, to account for ordering at a (typical) growth temperature ( $T_g$ ) of 900 K. When surface reconstructions are taken into account, however, we have shown<sup>5</sup> that the observed CuPt variant (on the surface there are two distinct variants of this structure,  $\text{CP}_A$  and  $\text{CP}_B$ , of which only the latter is observed) of  $\text{GaInP}_2$  is stabilized over other competing structures by almost 100 meV per surface atom. We find that the stability enhancement of the  $\text{CP}_B$  variant is intimately connected to novel dimer reconstructions. Similar calculations for  $\text{AlGaAs}_2$  surfaces produce only very small energy differences, in agreement with the experimental lack of ordering for  $\text{Al}_{0.5}\text{Ga}_{0.5}\text{As}$  on (001) substrates.

In this paper we discuss in detail the connection between the ordering in the surface layer, the surface reconstruction, and the surface electronic structure. We emphasize that all

our calculations are on monolayer-coverage cation-terminated surfaces using a  $2 \times 2$  unit cell.

## II. METHOD

Several common 3D structures can be obtained (Table I) by stacking the five prototype (001) alloy bilayers shown in Fig. 1. Since each of the surfaces can potentially reconstruct in many different ways, we will use the term topology to indicate the surface pattern, i.e., *a–e*, of the atoms on the surface and the word geometry to describe an actual atomic configuration or reconstruction for a given surface.

In order to compare the energies of these prototypes and obtain their minimum energy geometries, we used a repeated slab geometry. Two types of slabs were used. The first, which was used for most of the cation-terminated surfaces consisted of three atomic GaAs (substrate) layers covered on each side by single, cation-terminated bi-layers of GaInP<sub>2</sub> (or AlGaAs<sub>2</sub>) in the topologies *a–e* and separated by four empty layers. The bottom and top layers are kept identical to prevent spurious charge transfer. The second type was a “single-surface” slab with a Ga<sub>0.5</sub>In<sub>0.5</sub>P top surface and a GaAs bottom surface terminated by half a monolayer of Ga.<sup>12</sup> The bottom surface is semiconducting which again prevents charge transfer. The single-surface slab is computationally more expensive but it allows relaxations five layers below the surface and was used to check our results.

The first-principles local-density pseudopotential method<sup>13</sup> is used to calculate the total energies and quantum mechanical forces are used to find equilibrium geometries for each of the five surfaces. In order to make the calculations possible, we generated soft pseudopotentials using the method of Vanderbilt.<sup>14</sup> This allows us to use a planewave cutoff of only 10 Ry. The resulting lattice constants of the binaries, 5.45, 5.24, 5.80, and 5.61 Å for GaAs, GaP, InAs, and InP,

TABLE I. 3D structures characterized by stacking of the (001) bilayers shown in Fig. 1. The structures are identified both by a superlattice notation (the direction *G* and the repeat period  $2n$ ) and by the notation used in the text. Each layer is shifted laterally as indicated in parenthesis (in units of the zinc-blende lattice constant). Several other structures are degenerate with those tabulated:  $[110] n = 1$  is identical to  $[001] n = 1$  CA;  $[201] n = 2$  CH is degenerate with  $[021] n = 2$  CH; and  $[010]$  CA is degenerate with  $[100]$  CA. The  $[102] n = 2$  and  $[012] n = 2$  CH structures have (001) layers that cannot be represented by the  $2 \times 2$  patterns in Fig. 1. Notice that the *d* layer occurs only in the observed CP<sub>B</sub> phase and in the  $[1\bar{1}0] n = 2$  superlattice. The two are distinguished only by the third layer stacking.

Structure		Layer number			
<i>G, n</i>	Name	1	2	3	4
(binary)	<i>A</i>	<i>a</i> (0,0)	<i>a</i> (1/2,0)	<i>a</i> (0,0)	<i>a</i> (1/2,0)
(binary)	<i>B</i>	<i>b</i> (0,0)	<i>b</i> (1/2,0)	<i>b</i> (0,0)	<i>b</i> (1/2,0)
$[021], 2$	CH	<i>e</i> (0,0)	<i>e</i> (1/2,0)	<i>e</i> (1/2,1/2)	<i>e</i> (0,1/2)
$[100], 1$	CA	<i>e</i> (0,0)	<i>e</i> (1/2,0)	<i>e</i> (0,0)	<i>e</i> (1/2,0)
$[001], 1$	CA	<i>a</i> (0,0)	<i>b</i> (1/2,0)	<i>a</i> (0,0)	<i>b</i> (1/2,0)
$[111], 1$	CP <sub>A</sub>	<i>c</i> (0,0)	<i>c</i> (1/2,0)	<i>c</i> (1/2,1/2)	<i>c</i> (0, -1/2)
$[110], 2$	...	<i>c</i> (0,0)	<i>c</i> (1/2,0)	<i>c</i> (0,0)	<i>c</i> (1/2,0)
$[\bar{1}11], 1$	CP <sub>B</sub>	<i>d</i> (0,0)	<i>d</i> (1/2,0)	<i>d</i> (1/2, -1/2)	<i>d</i> (0,1/2)
$[\bar{1}10], 2$	...	<i>d</i> (0,0)	<i>d</i> (1/2,0)	<i>d</i> (0,0)	<i>d</i> (1/2,0)

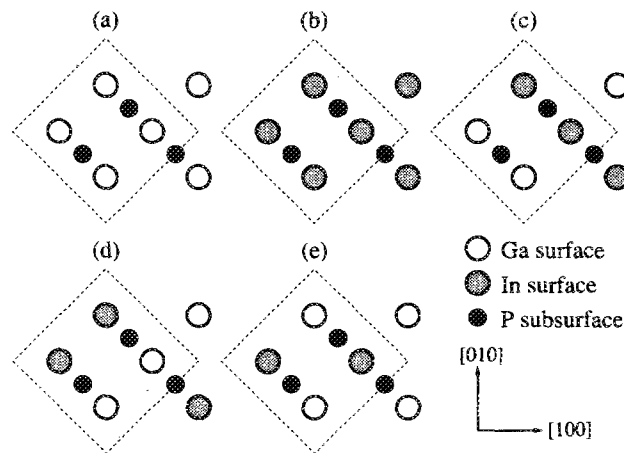


FIG. 1. Surface atomic arrangements for the  $2 \times 2$  surface cell. See Table I for description of corresponding bulk structures.

respectively, are about 4% smaller than experimental values. The deviation is, however, uniform so lattice-constant matches and/or mismatches are preserved. A 2D projection of the ten face-centered-cubic special *k* points<sup>15</sup> is used to perform the surface Brillouin zone integrals. We performed several tests in order to check that interactions between the two surfaces of our seven layer slab did not bias our results. (i) We added four additional layers of GaAs to the substrate and compared the two unreconstructed surfaces (*a + b* and *e*). The energy difference changed by less than 3 meV per surface atom. (ii) For the fully relaxed geometries, we shifted the upper half of the slab by one half the lattice constant of the surface unit cell and again energies changed by less than 6 meV. (iii) We fixed the atoms in the central layers of the slab in their ideal zinc-blende positions. Fixing one layer increased the energy of the *e* surface by 7 meV and fixing three layers raised the energy by 17 meV. (iv) Finally, we compared our results for the “normal” slab with those obtained using a “single-surface” slab. The energy difference between the fully relaxed *d* and *e* surfaces changed by less than 4 meV. Based on these tests, we estimate that energy differences between the various surfaces are accurate to better than 10 meV per surface atom.

## III. SURFACE GEOMETRIES AND RECONSTRUCTIONS

Calculated energies for relaxed but unreconstructed surfaces [Fig. 2(a)] are given in Table II, line 1. In agreement with the results of Boguslawski,<sup>11</sup> all unreconstructed surfaces (alloyed or phase separated) have energies that are equal within  $kT_g$ . Bulk calculations of strain energies for various ordered phases of GaInP<sub>2</sub> produce differences as large as 40 meV per pair of atoms<sup>16</sup> indicating that elastic size effects are better accommodated at surfaces than in the bulk. Presumably, this is because the surface atoms are free to relax in the direction perpendicular to the surface. Electronically, we find that all the unreconstructed surfaces are metallic.

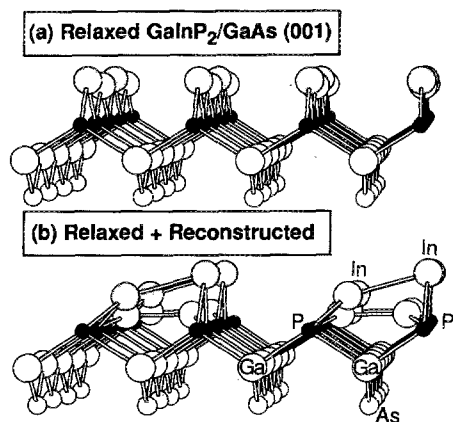


FIG. 2. Side view of relaxed atomic geometries for the  $d$  surface of  $\text{GaInP}_2$  on  $(001)\text{GaAs}$ . The surface atoms are Ga (white), In (grey), and P (black) on top of a GaAs substrate layer (white). Part (a) shows the relaxed but undimerized surface and part (b) the fully reconstructed surface with buckled and tilted dimers.

Surprisingly we find that the unreconstructed surfaces are unstable not only with respect to dimerization but also with respect to two additional reconstructions within the  $2 \times 2$  surface unit cell. First, neighboring dimers along the  $[\bar{1}10]$  dimer rows buckle, i.e., relax perpendicularly to the surface creating chains of alternate high and low dimers. This motion does not alter the symmetry of the  $d$  surface where the two dimers are already distinct before buckling, but it breaks the symmetry of the other surfaces. Second, the high dimer tilts in the  $[110]$  direction becoming nonhorizontal, with the low dimer remaining virtually horizontal. This tilt is natural for surfaces with heteropolar dimers ( $c$  and  $e$ ), but reflects symmetry breaking for the other surfaces. For the surfaces where the buckling or the tilting is not symmetry breaking the reconstruction can occur in two distinct ways obtained by interchanging the positions of the Ga and In atoms on the surface. The two types can be characterized by whether Ga or In is occupying the outermost or highest site. Because In is the larger atom, one might expect this site to be occupied by In but, as we shall see below, that is not always the case. The final minimum-energy surface geometry is illustrated in Fig. 2(b). As shown in Table II, the reconstructions (dimerization, buckling, and tilting) lower the energy of all the sur-

TABLE II. Surface energies for the unreconstructed (UR), and fully reconstructed with Ga up (DBT-1) and with In up (DBT-2) surfaces of  $\text{GaInP}_2$ . The energies are in meV per surface atom relative to the unreconstructed  $a + b$  phase-separated surface.

Surface geometry	Surface type			
	$a + b$	$c$	$d$	$e$
UR	0	14	-9	2
DBT-1	-701	-698	-623	-715
DBT-2	-701	-684	-799	-705

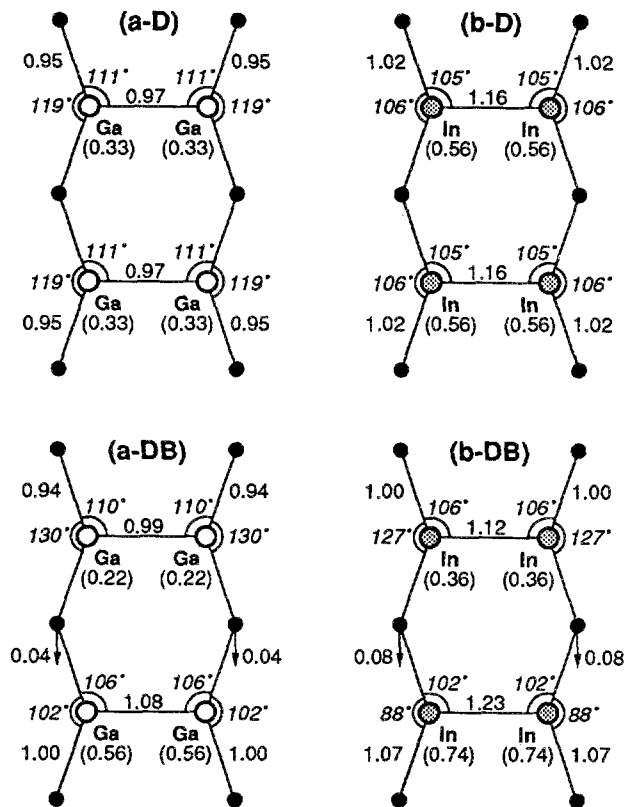


FIG. 3. Schematic top view of the  $2 \times 2$  unit cell depicting bond lengths and bond angles for the  $a$  and  $b$  surfaces with various reconstructions. Also given, in parenthesis, is the height of each Ga (white) and In (grey) atom over the P (black) subsurface layer and the approximate direction and magnitude of the horizontal displacement of the P atoms away from their ideal zinc-blende positions (we find that except for a common shift the vertical displacement of the P atoms is small). Parts (a-D) and (b-D) are dimerized only and (a-DB) and (b-DB) are dimerized and buckled. Lengths are given in units of the average of the bond lengths of bulk GaP and InP. In these units, the bulk bond lengths of GaP and InP are 0.96 and 1.04, respectively.

faces by an average of 700 meV per surface atom and, most significantly, make the surface corresponding to the observed  $\text{CP}_B$  order ( $d$ ) the lowest in energy by 84 meV per surface atom. All the fully reconstructed surfaces are semiconducting.

#### IV. SURFACE ELECTRONIC STRUCTURE

Since most previous calculations for  $(001)$  semiconductor surfaces have found simple symmetric dimers, it is perhaps useful to discuss the surface electronic structure in steps, including horizontal dimers and the fully reconstructed dimers. To illustrate the interplay between the geometric structural relaxation and the surface electronic structure, we will follow the surface states for the  $a$  and  $b$  surfaces (pure GaP and InP) as these surfaces dimerize, buckle, and finally tilt. Although similar results can be obtained for the other surfaces, the  $a$  and  $b$  surfaces were chosen because they can straightforwardly be prepared (theoretically) in each geometry. Our results are summarized in Table III, giving the total energies for the various reconstructions, in Figs. 3 and

TABLE III. Surface energies for the following reconstruction modes: dimerized (D), dimerized and buckled (DB), and dimerized, buckled, and tilted (DBT-1) (with Ga up) and (DBT-2) (with In up). The energies are in meV per surface atom relative to the unreconstructed surfaces (each surface has its own separate zero of energy).

Surface geometry	Surface type					
	<i>a</i>	<i>b</i>	<i>a + b</i>	<i>c</i>	<i>d</i>	<i>e</i>
D	-785	-366	-575	...	...	-621
DB	-732	-448	-590	...	-684	-604
DBT-1	-836	-564	-701	-712	-614	-717
DBT-2	-836	-564	-701	-698	-790	-706

4, tabulating the geometries, in Fig. 5, giving the energy levels of the surface states at  $\Gamma$ , and in Fig. 6 showing contour plots of actual states. Because we are dealing with a slab with two surfaces, the energy levels in Fig. 5 represent averages of two or more states and are only schematic. It should also be noted that every geometry with an entry in Table III represents a geometry where the calculated atomic forces are zero. This may be a local energy minimum as for the buckled *a* surface, or, possibly, an energy maximum for the unbuckled *b* surface. To form a (001) surface, we must break two bonds per surface atom. On a cation surface, each broken bond contributes 3/4 of one electron and there are four broken bonds per dimer. When the surface dimerizes, two electrons per dimer go into a low-energy bonding state. In Figs. 5 and 6 we denote this state  $p_\sigma$  although it also has some *s* character. The state is  $\sim 2$  eV below the Fermi level and is strongly localized along the dimer bonds. We are left with one electron per dimer making the dimerized surfaces metallic. This electron goes partly into a  $p_\pi$  bonding state and partly into an  $s + p_\pi$  antibonding state. We denote the latter *D* for its dangling bond appearance. On the *b* surface the  $p_\pi$  and *D* states are almost degenerate but on the *a* surface the more tightly bound Ga-Ga dimers cause the two states to split by  $\sim 0.5$  eV. The dimer buckling mainly affects the dangling bond states. The dangling bond state on the low dimer,  $D_l$ , becomes more *p*-like and increases in energy with respect to the dangling bond state on the high dimer,  $D_h$ , which becomes more *s*-like. The  $D_l$ - $D_h$  splitting is  $\sim 1$  eV for both surfaces. This causes a transfer of electrons from the low dimer to the high dimer upon buckling. Since the dangling bond state on the *a* surface was unoccupied, well above the  $p_\pi$  state, before buckling, the effect of buckling on the *a* surface is small and its surface energy actually increases. For the *b* surface, on the other hand, where the states were degenerate initially, the buckling leads to significant charge transfer and the total energy of the *b* surface decreases. Even for the *b* surface the splitting is insufficient, however, to produce a gap throughout the surface Brillouin zone and the surface remains metallic. Finally, the tilting of the high dimer strongly couples the  $D_h$  state and the  $p_{\pi h}$  bonding state creating a low-energy dangling bond state  $D_h^+$  on the raised atom and a  $p_z$  state, denoted  $D_h^-$ , on the lowered atom. At this point the splitting is large enough to cause full occupation of the  $D_h^+$  state leaving the remaining  $p_{\pi l}$ ,  $D_h^-$ , and  $D_l$  states

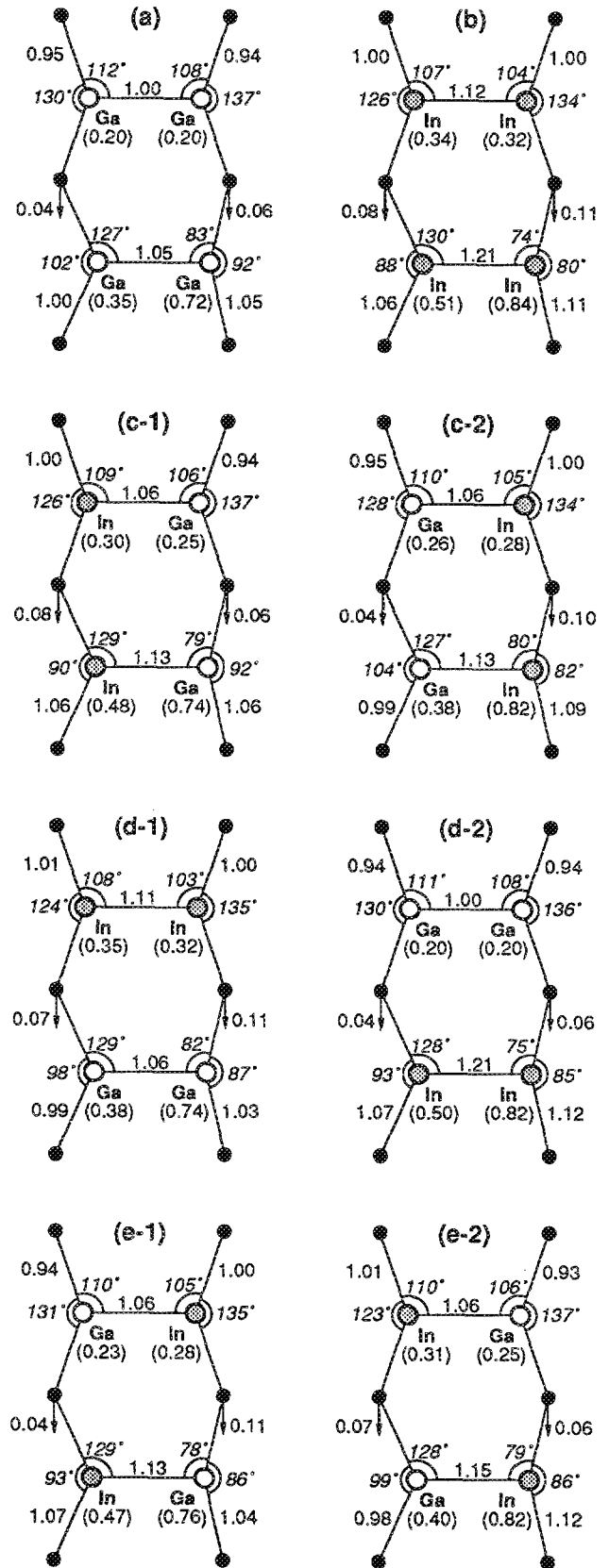


FIG. 4. Schematic top view of  $2 \times 2$  unit cell depicting fully relaxed and reconstructed geometries (dimerized, buckled, and tilted) for the five prototype surfaces shown in Fig. 1. For the surfaces *c*, *d*, and *e* we show the two variants with Ga up (1) and In up (2). The notation and units are defined in the figure caption of Fig. 3.

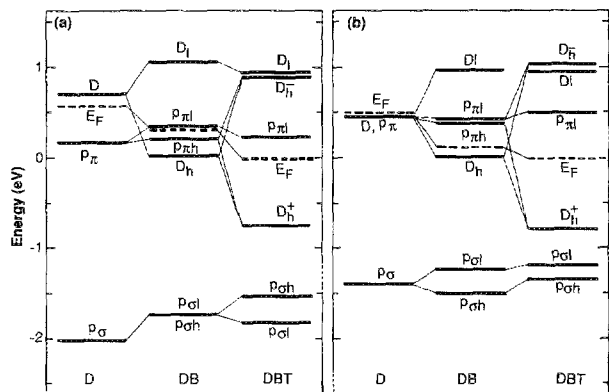


FIG. 5. Energy levels for selected surface states for surfaces *a* (GaP) and *b* (InP) in the following geometries: dimerized only (D), dimerized and buckled (DB), and dimerized, buckled, and tilted (DBT). The notation used for the states is described in the text. The zero of energy is chosen equal to the Fermi level in the DBT geometry.

empty. The buckled and tilted surfaces are all semiconducting. The final geometries depicted in Figs. 2(b) and 4 show that three of the four surface atoms are in approximate planar *sp*<sup>2</sup> bonding configurations and the fourth atom raises up into an *s*<sup>2</sup>*p*<sup>3</sup> configuration with 90° bond angles. Thus the raised atom acts as an anion accepting 1/2 electron from each of the other three cations. Counting the number of *s* and *p* electrons we see that the raised atom has one additional *s* and one additional *p* electron. Based on atomic orbital energies, Ga is the more electronegative surface atom for both the GaInP<sub>2</sub> and the AlGaAs<sub>2</sub> surfaces and we therefore expect that Ga will occupy the raised position. This is in agreement with our results for AlGaAs<sub>2</sub>, but only partially so for the GaInP<sub>2</sub> surfaces. For the latter the large size difference between Ga and In creates a preference for Ga as a low atom, particularly on the low dimer where the ideal *sp*<sup>2</sup> bonding arrangement is achieved when the cations are coplanar with the P subsurface atoms.

Table III also includes entries for other surfaces in the various stages of reconstruction. In all cases we see that a pair of simple dimers forms a “negative U” system where

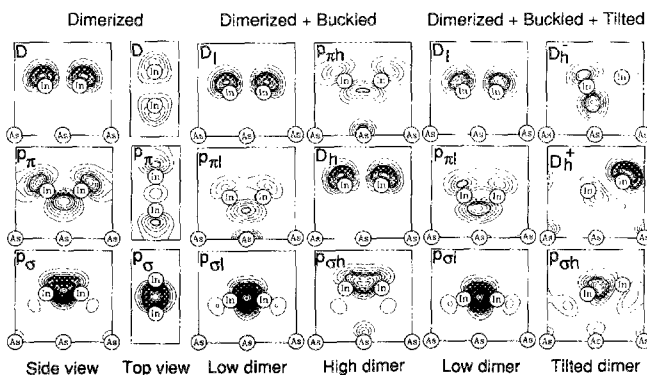


FIG. 6. Contour plots of selected surface states at  $\Gamma$  for the *b* surface in the following geometries: dimerized only (D), dimerized and buckled (DB), and dimerized, buckled, and tilted (DBT). The notation used for the states is described in text.

two neutral (horizontal) dimers are unstable with respect to disproportionation into a positively charged low dimer and a negatively charged high and tilted dimer.

V. DISCUSSION

By examining the entries in Table III, we see that the relative total energies are insensitive to the geometry of the high dimer. This suggests that the low dimer may be responsible for the increased stability of the *d* surface over the others. It is the only surface (among *a* + *b*, *c*, *d*, and *e*) where this dimer contains two small Ga atoms and therefore most easily can relax into the electronically optimal, bonding arrangement coplanar with the P atoms. This analysis suggests that if the two electrons in the dangling bond state *D*<sub>*h*</sub><sup>+</sup> (Fig. 6) on the high dimer could be removed, e.g., by heavy *p* doping or by excitation, both dimers would prefer planar *sp*<sup>2</sup> arrangements and the energy advantage of the *d* surface should vanish. Our calculations show that the energy difference between the *d* and *e* surfaces is indeed reduced to 1 meV per surface atom upon the removal of two electrons per surface unit cell. This is one possible reason why *p*-doped samples show reduced ordering.<sup>17</sup> If the cation surface coverage  $\theta$  is less than 3/4 monolayer, the high dimer dangling bond electrons can transfer to P dangling bonds. For 3/4 <  $\theta$  < 1, the transfer is partial. We would, therefore, expect the ordering to be reduced for surfaces with 3/4 <  $\theta$  < 1 and to vanish for  $\theta \leq 3/4$ .

VI. SUMMARY

Using the first-principles pseudopotential method, we have studied the energetics of several 2 × 2 surface atomic arrangements for a single Ga<sub>0.5</sub>In<sub>0.5</sub>P layer on a GaAs substrate. We find that among the fully relaxed, dimerized Ga<sub>0.5</sub>In<sub>0.5</sub>P surfaces, the surface corresponding to the observed CuPt-like 3D order is favored over the closest competing surface by ~100 meV per surface atom. For the Al<sub>0.5</sub>Ga<sub>0.5</sub>As control surfaces, we do not find that a single surface arrangement of atoms is preferred. The reconstruction pattern for all these fully covered 2 × 2 cation-terminated surfaces is the same; one symmetric dimer close to the surface, and one tilted dimer which moves up, away from the surface. These novel reconstruction modes, which are electronically driven and allows the monolayer-covered cation-terminated surfaces to be semiconducting. For ionized surfaces or partially covered surfaces, the additional reconstruction modes are not present and the stability enhancement vanishes.

<sup>1</sup> D. K. Biegelsen, R. D. Bringans, J. E. Northrup, and L.-E. Swartz, Phys. Rev. B **41**, 5701 (1990).  
<sup>2</sup> M. D. Pashley, Phys. Rev. B **40**, 10481 (1989).  
<sup>3</sup> J. N. Baillargeon, K. Y. Cheng, and K. C. Hsieh, Appl. Phys. Lett. **56**, 2201 (1990).  
<sup>4</sup> G.-X. Qian, R. M. Martin, and D. J. Chadi, Phys. Rev. B **38**, 7649 (1988).  
<sup>5</sup> S. Froyen and A. Zunger, Phys. Rev. Lett. **66**, 2132 (1991).  
<sup>6</sup> See, e.g., S. C. Wu, S. H. Lu, Z. Q. Wang, C. K. C. Lok, J. Quinn, Y. S. Li, D. Tian, F. Jona, and P. M. Marcus, Phys. Rev. B **38**, 5363 (1988).  
<sup>7</sup> T. Suzuki, A. Gomyo, and S. Iijima, J. Cryst. Growth **93**, 396 (1988).  
<sup>8</sup> A. Gomyo, T. Suzuki, and S. Iijima, Phys. Rev. Lett. **60**, 2645 (1988).

- <sup>9</sup>R. G. Dandrea, J. E. Bernard, S.-H. Wei, and A. Zunger, *Phys. Rev. Lett.* **64**, 36 (1990).
- <sup>10</sup>J. E. Bernard, L. G. Ferreira, S.-H. Wei, and A. Zunger, *Phys. Rev. B* **38**, 6338 (1988); J. E. Bernard, R. G. Dandrea, L. G. Ferreira, S. Froyen, S.-H. Wei, and A. Zunger, *Appl. Phys. Lett.* **56**, 731 (1990).
- <sup>11</sup>P. Bogusławski, *Phys. Rev. B* **42**, 3737 (1990).
- <sup>12</sup>We used a checkerboard  $2 \times 2$  vacancy pattern instead of the  $2 \times 1$  pattern used by D. J. Chadi, *J. Vac. Sci. Technol. A* **5**, 834 (1987).
- <sup>13</sup>J. Ihm, A. Zunger, and M. L. Cohen, *J. Phys. C* **12**, 4409 (1979).
- <sup>14</sup>D. Vanderbilt, *Phys. Rev. B* **32**, 8412 (1985).
- <sup>15</sup>S. Froyen, *Phys. Rev. B* **39**, 3168 (1989). We used the generating vectors  $f_0 = 2\pi/a(1/8, 1/8, 0)$ ,  $f_1 = 2\pi/a(1/4, 0, 0)$ ,  $f_2 = 2\pi/a(0, 1/4, 0)$ ,  $f_3 = 2\pi/c(0, 0, 1)$ , where  $a$  is the alloy lattice constant and  $c$  is the thickness of the slab plus vacuum.
- <sup>16</sup>J. E. Bernard, L. G. Ferreira, S.-H. Wei, and A. Zunger, *Phys. Rev. B* **38**, 6338 (1988).
- <sup>17</sup>S. Kurtz, J. M. Olson, J. P. Goral, A. Kibbler, and E. Beck, *J. Electron. Mater.* **19**, 825 (1990).